Study of Aspect Ratio Effects on Kinetic MHD Instabilities in NSTX and DIII-D

E.D. Fredrickson,[a] W.W. Heidbrink,[b] C.Z. Cheng,[a] N.N. Gorelenkov,[a] E. Belova,[a]
A.W. Hyatt,[c] G.J. Kramer,[a] J. Manickam,[a] J. Menard,[a] R. Nazikian,[a] T. L. Rhodes,[d]
E. Ruskov[b]

[a] Princeton Plasma Physics Laboratory, NJ
[b] University of California, Irvine, CA
[c] General Atomics, La Jolla, CA
[d] University of California, Los Angeles, CA

e-mail contact of main author: efredrickson@pppl.gov

Abstract. We report general observations of kinetic instabilities on the low aspect-ratio National Spherical Torus Experiment (NSTX) and describe explicit aspect ratio scaling studies of kinetic instabilities using both the NSTX and the DIII-D tokamak. The NSTX and the DIII-D tokamak are nearly ideal for such experiments, having a factor of two difference in major radius but otherwise similar parameters. We also introduce new theoretical work on the physics of kinetic ballooning modes (KBM), toroidal Alfvén eigenmodes (TAE), and compressional Alfvén eigenmodes (CAE) with applications to NSTX.

1. Introduction

A wide range of kinetic instabilities is seen on NSTX. NSTX operates in a relatively new fast-ion parameter regime combining low aspect ratio with a large population of fast ions, produced by high-power neutral beam injection, well above the Alfvén speed, $1 < v_b/v_A < 3$ (where v_b is the beam ion speed and v_A is the Alfvén speed). This is similar to the regime expected on ITER where $1 < v_\alpha / v_A < 2$, and v_α is the alpha birth velocity. It is important to understand the relative importance of low aspect-ratio *vs*. the *trans*-Alfvénic fast ion population in exciting these instabilities. The DIII-D tokamak can provide plasma parameters similar in every way to NSTX, with the exception that the aspect ratio is larger. A similarity study of the toroidal Alfvén eigenmode (TAE) shows that the toroidal mode numbers scale as expected, supporting an expectation of a "sea" of unstable modes in a reactor. Kinetic instabilities with frequencies that chirp rapidly are common in NSTX but rare in DIII-D. Efforts to understand this difference in terms of the hole-clump theory of Berk and Breizman are reported. Compressional Alfvén modes (CAE) on NSTX have a frequency scaling, polarization, dependence on the fast-ion distribution function, and low frequency limit which are qualitatively consistent with CAE theory. Experiments are planned to compare the stability limits on DIII-D with those on NSTX to determine if CAE will be excited by alphas in a reactor. Theoretical work has found new insights into the ballooning instability. We show that the combined kinetic effect of trapped-electron dynamics and large ion Larmor-radii produces a large parallel electric field and hence a parallel current that greatly enhances the stabilizing effect of field line tension.

2. Aspect-Ratio Scaling of Toroidal Alfvén Eigenmodes

As in normal aspect-ratio tokamaks, TAEs [1] are destabilized in NSTX when the fast-ion velocity (v_b) is larger than V_A. The TAE can appear either as saturated modes, or as bursting modes in the frequency range 50 - 150 *kHz*. The bursting TAEs observed in NSTX [2] can cause significant fast ion losses. For NSTX shot 108530 shown in Fig. 1, the toroidal mode-numbers of the observed TAEs are $n = 2 - 5$. The mode frequency increases with n with

roughly equal frequency spacing. The mode growth rate, in the presence of multiple bursts and multiple modes, varies between $\gamma/\omega_{TAE} \approx 1.6 \times 10^{-3}$ and $\approx 6 \times 10^{-3}$ ($\omega_{TAE} \approx v_A / 2qR$, where V_A is the Alfvén velocity). The TAE bursts eject the fast ions, driving the mode, thereby lowering the growth rate, but the presence of multiple modes may non-linearly enhance the growth rate. In NSTX the TAE appear more often when q(0) > 1.5 (inferred from EFIT [3]). As predicted, modes at the higher gap frequencies have not yet been observed.

The observations of TAE are consistent with theory developed for normal aspect ratio tokamaks. At low aspect ratio, the Alfvén continuum gap is broad and NOVA-K [4] analysis predicts a broad TAE spectrum with many toroidal mode numbers (*n*). Plasma toroidal rotation Doppler-shifts the frequencies, affecting the resonance interaction between TAEs and particles and greatly modifying the mode stability. The calculated linear growth rates are $\gamma/\omega \approx 10^{-2}$ for a beam beta, $\beta_b \approx 1 - 3\%$, and the frequencies of the unstable modes are
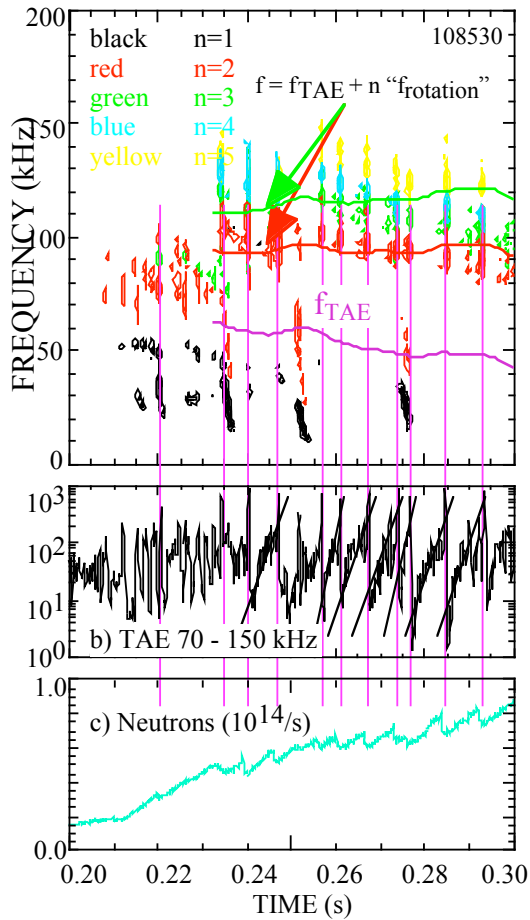
consistent with the observations. NOVA-K has predicted that plasmas with high q(0) will be more unstable to TAE and that β does not close the toroidicity-induced gap, but does close the ellipticity-induced and other higher gaps, consistent with the experimental observations [5].

The linear theory predicts that the range of unstable *n's* is determined by the fast ion finite orbit-width (FOW) effect. The fast ion drive is maximum in the range $n_{min} < n < n_{max}$, where $n_{min} \approx rn_{max}/ R$, $n_{max} \approx r\omega_{cf}/q^2 v_A$, and ω_{cf} is the fast ion cyclotron frequency. The *n* range of the most unstable TAEs shifts toward higher *n*'s at lower q and in larger devices such as ITER. This range has been verified by NOVA-K code calculations with FOW and finite Larmor-radius, ρ effects included.

The analytic scaling of the least stable *n* was tested in the NSTX and DIII-D. Both devices can operate with similar magnetic field, current density and temperature. Further, the most important dimensionless parameters for Alfvén mode stability, v_b/v_A and the normalized fast-ion pressure, β_b, are similar in the two devices. In addition, the cross-sectional shapes of the plasma can be closely matched. Thus, it is possible to study MHD and kinetic instabilities with all plasma parameters closely matched, except the major
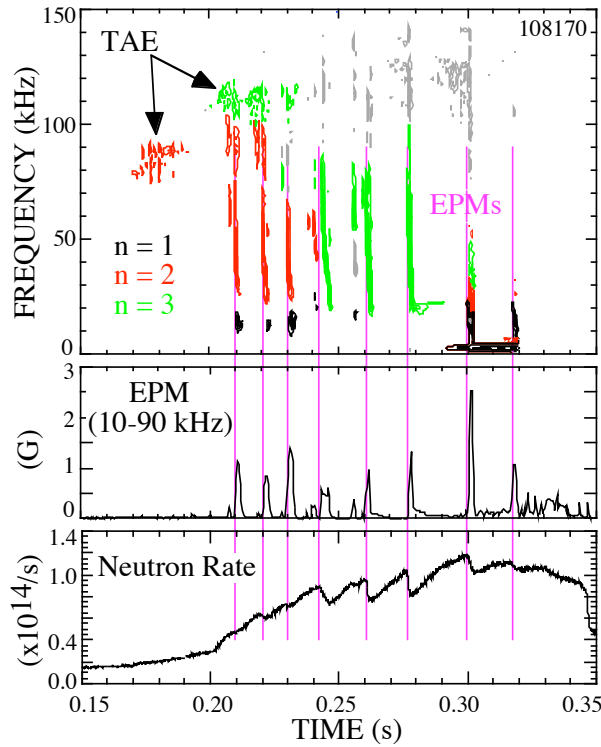

Fig. 1 TAE-induced fast ion losses. In the top panel is shown the spectrum of a Mirnov coil: black is n = 1, red is n = 2, green is n=3, blue is n=4, and yellow is n=5. The solid lines show the approximate Doppler-shifted TAE frequencies.b) RMS amplitude in mG of magnetic fluctuations between 70 and 150 kHz (TAE), c) total neutron production rate showing drops at TAE bursts.

radius, which differs by a factor of two. In practice, however, there are differences in the *q* profile between the two devices. In the similarity experiments, TAEs are observed with *n* = 1 − 2 in NSTX, whereas *n* = 2 − 7 in DIII-D. We have analyzed these experiments employing the NOVA and NOVA-K codes and recovered the observed scaling [6,7].

Fig. 2   EPM-induced fast ion losses. In the top panel is shown the spectrum of a Mirnov coil: black is n = 1, red is n = 2, green is n=3. b) rms amplitude in G of magnetic fluctuations between 10 and 90 kHz (TAE), c) total neutron production rate showing drops at EPM bursts.

2. Energetic Particle (Chirping) Modes

Bursting modes, which exhibit rapid downward frequency shifts (chirping) during each burst, Fig. 2, are a characteristic feature of energetic particle modes (EPM). The modes can chirp because the frequency is determined by the fast-ion distribution function, which can be directly modified by the modes, rather than parameters of the thermal plasma. Such modes are common in NSTX plasmas heated with neutral beams [8]. The modes qualitatively resemble the fishbone instability, a type of EPM, discovered on PDX [9], but have significant differences. In particular, the modes can have $n \geq 2$ and can be present when $q(0) > 1$. The most significant difference is that the NSTX EPMs can be driven through a fast-ion bounce resonance, rather than the fast-ion precession-drift resonance as in the PDX fishbone instability. The low field and large aspect-ratio of NSTX results in a bounce frequency, f_b only a little larger than the precession drift frequency, f_p since the ratio of bounce frequency, for deeply
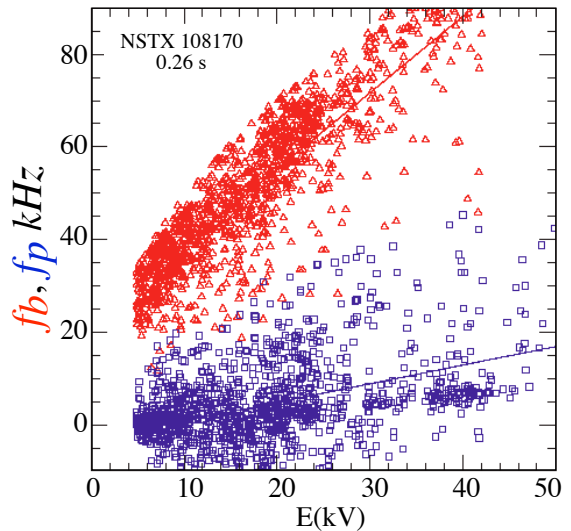
trapped ions, to precession frequency scales as:

$$\frac{f_b}{f_p} \propto \frac{r}{q^2 \rho_b} \sqrt{\frac{2r}{R}} ,$$

where ρ_b is the beam ion Larmor radius. While the precession-drift resonance could excite EPMs under some conditions in NSTX, often the precession frequency becomes small or negative in the latter periods of NSTX discharges similar to the situation predicted for ITER (Fig. 3). The bounce-resonance drive becomes most important at low shear and high $q(0)$, the conditions desired for an ST (or advanced tokamak) reactor.

Fig. 3. Trapped particle bounce (red) frequency (f_b) and precession (blue) frequency (f_p) for representative NSTX conditions.

While drops in the neutron rate approaching 40% are seen with some fishbone events [2], in many cases the neutron rate is essentially unaffected (Fig. 2c). The large neutron-rate drops indicate the loss from the plasma of a substantial fraction of the most energetic fast ions which are responsible for most of the neutron production. Smaller neutron-rate drops could indicate either that the fast ions are just redistributed within the plasma, or that only the lower energy fast ions are expelled.

Large fast ion losses are seen in many NSTX shots correlated with TAE and fishbone bursts. It is important to understand the scaling of these losses with respect to NSTX parameters, as well as inter-machine parameters such as aspect ratio. Preliminary scaling studies on NSTX have found no evidence that operation at high beta or high current will ameliorate the losses. In Figs. 4a – 4c, the loss fraction (% drop in neutron rate) for many discrete "events" is shown vs. toroidal field, plasma current and beta. As can be seen, the maximum loss fraction does not depend strongly on any of these parameters.
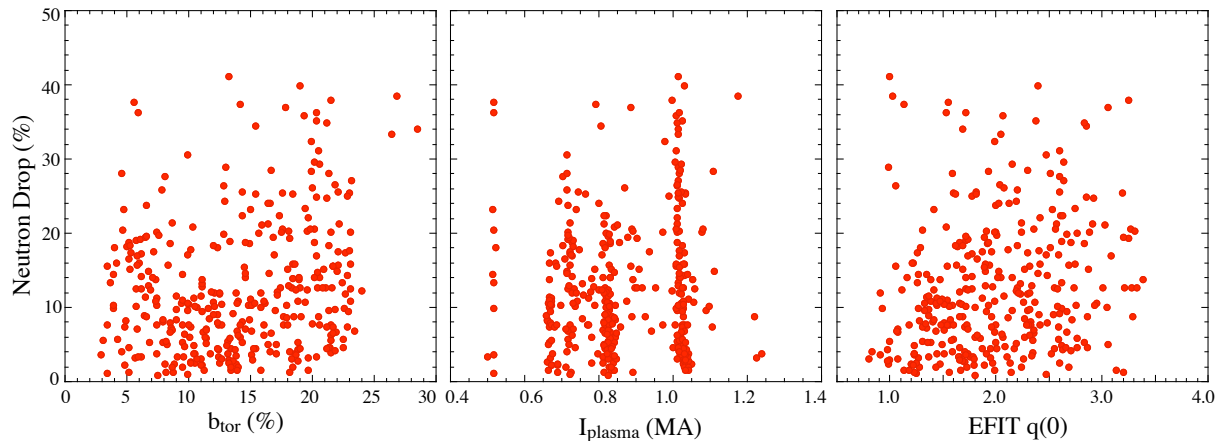

Fig. 4. Change in neutron rate during TAE, fishbone or combined TAE/fishbone bursts on NSTX.

While instabilities with frequencies that chirp rapidly are common in NSTX [5], they are rare in DIII-D [10]. It is important to develop a theoretical understanding of which of the parameters that differ between DIII-D and NSTX (*e.g.,* ρ_b/r, r/R, ...) are important in EPM stability. A theory by Berk and Breizman [11] suggests that chirping occurs when perturbations in the fast-ion phase space (a hole-clump pair) are preserved throughout the evolution of the instability. The absence of chirping in DIII-D may be because the particularly effective beam-ion transport in DIII-D [10,12] rapidly destroys the hole-clump pair, suppressing chirping. An experiment on NSTX attempted to spoil the chirping phenomenon by raising the effective collisionality of the resonant fast ions. High harmonic fast wave (HHFW) heating [13], which primarily heats electrons, can also heat the fast beam ions. The heating of the beam ions might effectively enhance the fast ion diffusion in velocity (phase) space, mitigating the chirping. Unfortunately, HHFW was found to be ineffective in controlling the frequency chirping. However, in the early part of the discharge the HHFW was found to stabilize the TAE.

3. Aspect-Ratio Scaling of Compressional Alfvén Eigenmodes

Compressional Alfvén Eigenmodes (CAEs) [14] and Global Alfvén Eigenmode (GAEs) [15,16] in the sub-ion-cyclotron frequency range are commonly excited during NBI in NSTX (Fig. 5) [17]. The toroidal mode numbers of the CAE have been measured for a few cases and are in the range $6 \leq n \leq 12$ and the polarization of the modes, measured at the vacuum vessel wall,
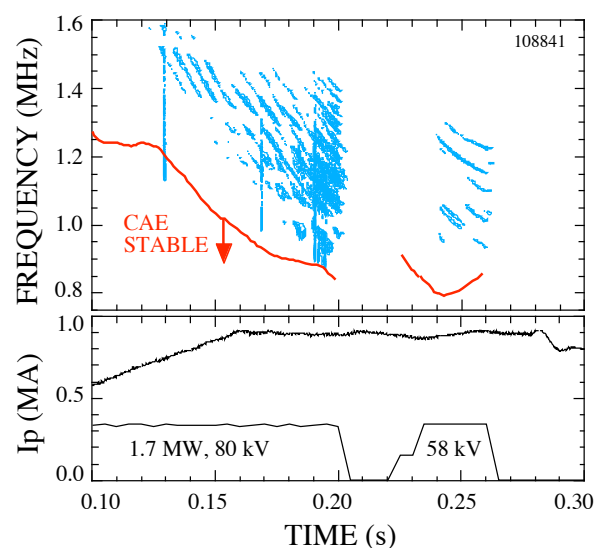

Fig. 5. Spectrogram of Mirnov coil signal showing CAE activity. Red line show theoretical minimum frequency. Lower panel shows plasma current evolution and neutral beam injection heating power.

is consistent with compressional waves. Many modes are present simultaneously and the spectrum typically shows a hierarchy of peaks, with evenly spaced large peaks, flanked by more closely spaced smaller peaks (*c.f.,* Fig. 8).
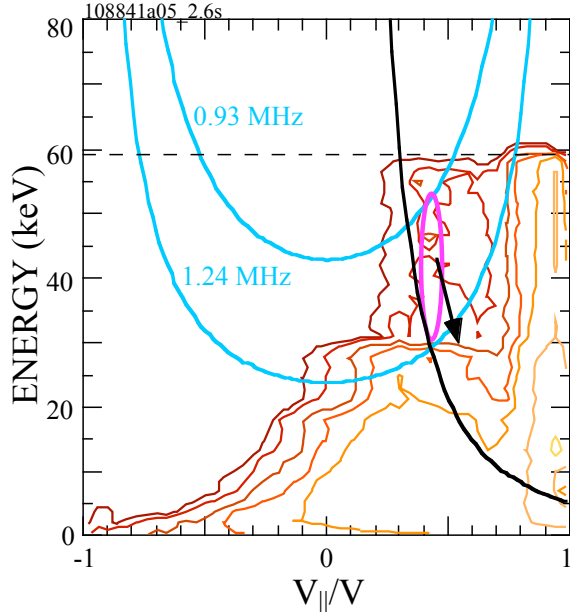

Fig. 6.   Fast ion distribution function as calculated in TRANSP. CAE activity between ≈ 0.93 and ≈ 1.24 MHz was seen in this shot. The blue curves indicate the $k_\perp\rho = 1$ constraint for the minimum and maximum frequencies, respectively.   The black arrow indicates the trajectory of a fast ion as it loses perpendicular energy to the CAE.

The fast ion distribution calculated by the beam deposition code in TRANSP [18] is shown in Fig. 6 (outboard midplane, $0.6 \le r/a \le 0.8$). The mode excitation in NSTX is predicted to be through a Doppler-shifted ion-cyclotron resonance [19]

$$\omega = \omega_{cb} - k_\theta v_{drift} - k_\| v_{b\|}$$

with the fast ions in the bump-on-tail in the perpendicular direction highlighted by the magenta oval (ω_{cb} is the beam ion gyrofrequency, v_{drift} is the curvature drift, and $v_{b\|}$ is the beam ion parallel velocity). The ion-cyclotron resonance takes mostly perpendicular energy, moving the fast ions in the direction of the black arrow, down the gradient. Only the fast ions above, and to the right, of the black curve have sufficient parallel energy to satisfy the resonance condition. The experimentally observed minimum frequency for CAE is found to be consistent with the prediction that the fast-ion

drive becomes weak for $k_\perp \rho > 1$ (red curve, Fig. 5).   This constraint is also indicated in Fig. 6 by the two blue curves covering the range of observed CAE frequencies. Fast ions above the blue curves have sufficiently large Larmor radius to satisfy the $k_\perp \rho > 1$ constraint. From the above analysis, the calculated fast-ion distribution function is found to be *qualitatively* consistent with the constraints of the Doppler-shifted ion cyclotron resonance model.

A numerical code, which solves the simplified dispersion relation for CAE [20-23], is used in the planning of experiments and interpretation of the results. For illustration, the equation in cylindrical geometry is:

$$\left\{ \frac{1}{r}\frac{\partial}{\partial r} r \frac{\partial}{\partial r} + \left[\left. \frac{\omega^2}{v_A^2} - \frac{n^2}{R^2} \right|_{\substack{outer \\ midplane}} - \frac{m^2}{r^2} \right] \right\} f_r = 0$$

The part of this equation in square brackets forms a radial well, but one whose shape depends on the eigenvalues (ω and m) of the mode. In toroidal geometry, particularly at low aspect-ratio, this well becomes asymmetric, tending to localize the wave amplitude to the outboard midplane. The aspect ratio, the shape of the density profile, and the poloidal and toroidal mode-numbers all influence the degree
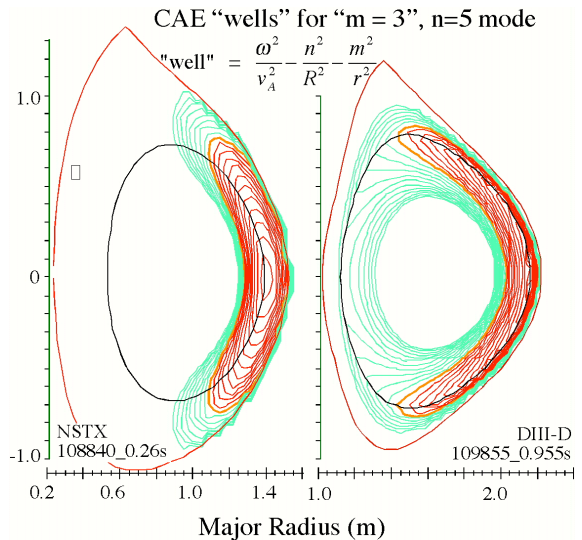

CAE "wells" for "m = 3", n=5 mode

$$\text{"well"} = \frac{\omega^2}{v_A^2} - \frac{n^2}{R^2} - \frac{m^2}{r^2}$$

Fig. 7. Calculated CAE "wells" for DIII-D and NSTX (NSTX figure is inverted).

of mode localization. In Fig. 7 are shown two wells as calculated for relatively similar DIII-D and NSTX discharges (the NSTX shot was actually a *lower* single-null, and the cross-section is inverted in Fig. 7). Note that in the lower aspect-ratio NSTX shot, the well is more localized towards the outboard midplane.
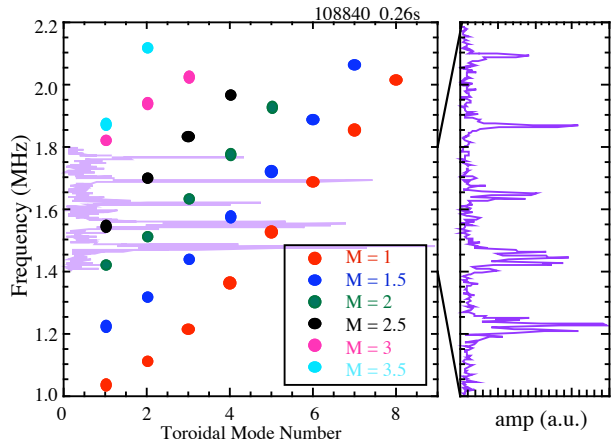

Fig.8. a) Predicted mode frequencies for $1 \leq n \leq 8$ and $1.5 \leq M \leq 3.5$. b) spectrum at time of analysis.

The frequency scaling of the modes agrees qualitatively with the predictions of this simple code, but the detailed structure of the spectrum is not captured with the simple model. In Fig. 8 are shown the predicted frequencies for the discrete modes with toroidal mode numbers $1 \leq n \leq 8$ and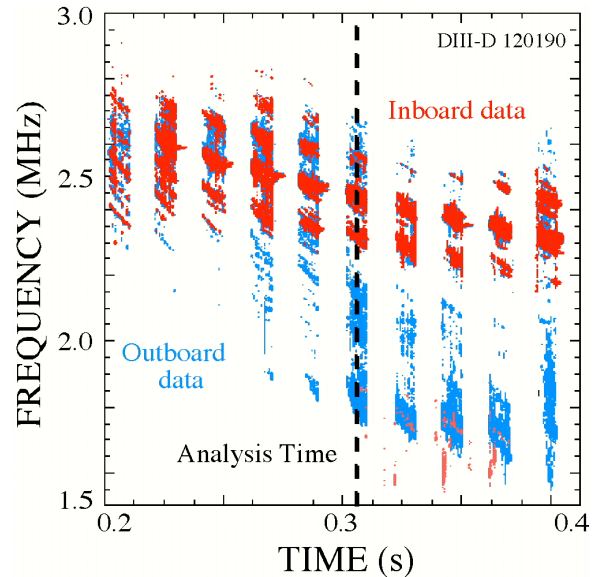 $1.5 \leq M \leq 3.5$ (where, *e.g.*, $M = 0.5$ is the lowest poloidal eigenmode). For higher M, the well opens up and the waves become propagating, making the M and $M + 0.5$ eigenmodes degenerate in frequency (note the mode frequencies at $M = 3$ and $M = 3.5$). The frequency spacing with M or n is comparable to the dominant spacing of the peaks in Fig. 8b, but not to the finer frequency splitting.

In experiments on DIII-D in which NSTX parameters were reproduced, CAE-like modes were seen [6]. An example is shown in Fig. 9 where a spectrogram from an inboard midplane sensor (red) is overlaid on the outboard midplane sensor spectrogram (blue). Modes above ≈ 2.2 MHz are seen on both sensors; below ≈ 2.2 MHz the modes are only seen on the outboard sensor, suggesting the modes are poloidally localized to the outboard

Fig. 9. Spectrograms of inboard and outboard midplane sensors, with inboard (red) overlaid on outboard (blue). DIII-D shot 120190.

side. The numerical calculations find that CAE exist at both low and high aspect ratio, but that the transition to poloidally propagating waves occurs at somewhat smaller poloidal mode numbers on DIII-D. For low poloidal mode numbers, the modes are predicted to be localized to the outboard side, similar to predictions for NSTX, but at higher M's (frequencies) the well is more poloidally symmetric. Interestingly, near the transition from poloidally localized to poloidally symmetric, the mode amplitude is predicted to peak on the inboard side. In Fig. 10 are shown the predicted frequencies for CAE *vs* poloidal and toroidal mode numbers. Closed symbols indicate modes where the

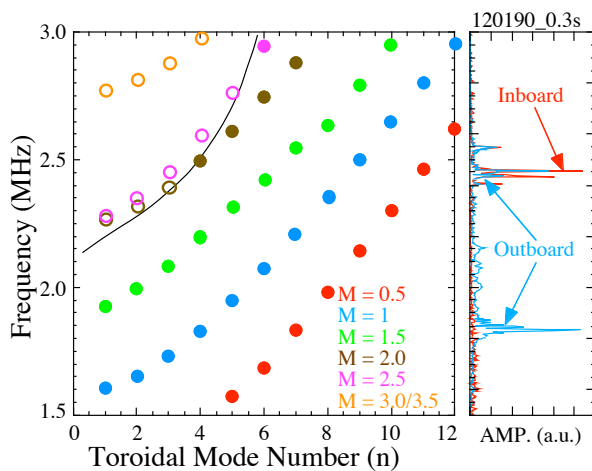*Fig. 10. Calculated mode frequencies for $1 \leq n \leq 12$ and $0.5 \leq M \leq 3.5$ compared to spectrum for DIII-D shot 120190 at 0.305s.*

poloidal well is closed on the inboard side (the wave becomes evanescent); open symbols indicate the modes where the radial well is poloidally open. The simulations predict that for modes below ≈ 2.2 MHz, the well is closed on the inboard side, in qualitative agreement with the data shown in Fig. 9.

GAEs are global modes dominated by one poloidal harmonic and their frequencies are just below the minimum of the Alfvén continuum $\omega^2_A(r)$ $(= k_\parallel^2 v_A^2)$. The mode is localized at the minimum of $\omega^2_A(r)$, which occurs at $r = 0$, for the typical flat q profiles in NSTX. The linear theory predicts unstable GAEs for $2 < (\omega / \omega_{cb}) (v_{\perp b0} / v_A) (k_\perp /k_\parallel) < 4$ (ω_{cb} is the beam ion gyrofrequency), where the bump-on-tail width in $v_\perp$ satisfies $\delta v_{\perp b} < 2 v_A \omega_{cb} /\omega$. While evidence for GAE has been found on NSTX [24], none has been found on DIII-D so far.

Much more advanced simulations were performed to study GAEs and CAEs in NSTX using the 3D hybrid HYM code [25], which treats beam ions using full-orbit, delta-f particle scheme and the thermal plasma using resistive MHD model. The initial equilibria are obtained by solving a generalized Grad-Shafranov equation which includes the beam-ion toroidal and poloidal currents [25]. Simulation results show that for $V_b > 3V_A$ many CAE/GAE with different n are excited. For $2 < n < 7$ the modes are mainly GAEs, which are localized near the magnetic axis and have large $k_\parallel$ (with $nm < 0$), so that $\omega \approx |k_\parallel V_\parallel| \approx 0.5\omega_{cb}$. For these modes $\delta B_\parallel \approx 1/3 \, \delta B_\perp$ due to strong coupling to the compressional Alfvén wave. For each n, several GAE modes with different m are unstable. Linearized simulations for different n show that $n + m \approx 6$ is satisfied (i.e. approximately same $k_\parallel$) for the most unstable modes. For a ratio of beam ion to plasma density, $n_b / n_p = 0.03$ and beam energy $E_b = 80$ keV, the GAE growth rates are $\gamma \approx (0.002 - 0.01)\times\omega_{ci}$ and frequencies $\omega \approx (0.3 - 0.5)\times\omega_{ci}$. Nonlinear simulation results show that GAEs saturate at low amplitudes with $\delta B/B = 10^{-4} - 10^{-3}$. For larger n (> 7), CAEs are the dominant modes with $\delta B_\parallel > \delta B_\perp$ and their growth rates are $\gamma \approx 0.001\times\omega_{ci}$. Unlike GAEs, CAEs are found to be localized on the low-field side, and have small $k_\parallel$ (with $nm >0$).

4. Kinetic Ballooning Modes

The ballooning instability results from the release of free energy of non-uniform pressure that has a gradient in the same direction as the magnetic field curvature. However, the kinetic effects of trapped electron dynamics, finite ion Larmor radii and wave-particle resonances are important in determining its stability. By considering $v_e >> \omega/k_\parallel >> v_i$, where $v_{e,i}$ are the electron and ion thermal velocities, respectively, we have shown that the combined kinetic effect produces a large parallel electric field and hence a parallel current, which greatly enhances the stabilizing effect of field line tension [26]. The stabilizing kinetic effect increases the first stability critical-β (β_c) and reduces the second-stability β_c over the MHD prediction by a factor proportional to n_e/n_{eu}, where n_e is the total electron density and n_{eu} is the untrapped electron density. For low aspect-ratio devices such as NSTX, we expect the stabilizing effect to be significant because $n_e/n_{eu} >>1$.

Fig. 11 The β_{cr} for the KBM and MHD ballooning mode (n = 12). Also shown are the NSTX β and q profiles.

We have computed the Kinetic Ballooning Mode (KBM) stability [26] for an NSTX equilibrium which has a moderate reverse shear, with q_{min} located at $\rho \approx 0.3$ [$\rho^2 = \Psi_{tor}(r)/\Psi(a)$]. Other parameters are: major radius $R = 0.86m$, minor radius $a = 0.68m$

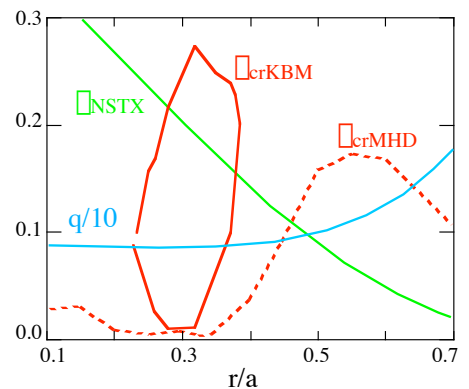(R/a!=!1.26), ellipticity   *1.63*, triangularity 0.417, and vacuum magnetic field B_0!=!*0.3T*. Figure 11 for zero temperature gradient shows that while MHD ballooning modes are unstable for *0.05 < ρ < 0.45,* the KBMs are unstable only near q_{min} *(0.28 < ρ < 0.37 for n = 12)*. The KBM real frequency is less than the ion diamagnetic-drift frequency, ω_{*i}, but its growth rate is much smaller than the MHD ballooning-mode growth rate. At *R/a = 1.67,* KBMs are unstable in a larger radial domain *(0.28 < ρ < 0.44)* mainly because n_e/n_{eu} is smaller at larger *R/a*.

Allowing finite ion and electron temperature gradients (choosing $\eta_i =$ $\eta_e = 1$ for all minor radii in the same NSTX equilibrium), the stability boundary in the (β, r/a) domain is modified with the first β_c increased slightly, but the second β_c increased greatly due to the coupling between the KBM and the η_i mode. However, the unstable radial domain is *0.35!>!r/a!>!0.27,* similar to the zero temperature gradient case. Near marginal stability the KBM real frequency is larger than $(1+!\eta_i)\omega_{*i}$. For an equilibrium with a slightly larger aspect ratio (*R/a = 1.67*) than the baseline NSTX case (*R/a!=!1.26*), KBMs are unstable in a larger radial domain (*0.28!<!r/a!<!0.44*) mainly because it requires larger minor radii for the stabilizing influence of trapped electrons to become effective in a larger aspect-ratio device.

5. Acknowledgements

6. References

[1]   C.Z. Cheng and M.S. Chance, Phys. Fluids **29**, (1986) 2471.
[2]   E.D. Fredrickson, N N Gorelenkov, D Darrow, *et al.*, Phys. of Plasmas **10** (2003) 2852.
[3]   S A Sabbagh, S M Kaye, J E Menard, *et al.*, Nucl. Fusion **41**, 1601 (2001).
[4]   C. Z. Cheng, Phys. Reports **211**, 1-51 (1992).
[5]   N.N. Gorelenkov, C.Z. Cheng, G-Y. Fu, et al.,Phys. of Plasmas **7** (2000) 1433.
[6]   W.W. Heidbrink, ED Fredrickson, N N Gorelenkov, *et al.*, Plas. Phys. Cont. Fus. **45** (2003) 983.
[7]   N.N. Gorelenkov, E.V. Belova, H.L.Berk, C.Z. Cheng, *et al.,* Phys. Plasmas 11 (2004) 2586.
[8]   E.D. Fredrickson, L Chen, R B White, Nucl. Fusion **43** (2003) 1258.
[9]   K. M. McGuire, R. Goldston, M Bell, et al., Phys. Rev. Lett. **50** 891 (1983).
[10] W.W. Heidbrink, Plasma Physics and Controlled Fusion **37** (1995) 937.
[11] H.L. Berk, B.N. Breizman, J. Candy, *et al.*, Phys. Plasmas **6** (1996) 3102.
[12] E.M. Carolipio, W.W. Heidbrink, C. Z. Cheng, *et al.,* Phys. Plasmas **8** (2001) 3391.
[13] A. L. Rosenberg,b) J. E. Menard, J. R. Wilson, *et al.,* Phys. Plasmas **11** (2004) 2441.
[14] N N Gorelenkov, C Z Cheng, E Fredrickson, *et al.,* Nucl. Fusion **42** 977 (2002).
[15] K Appert *et al.,* Plasma Phys., **24** 1147 (1982).
[16] J.W. Van Dam *et al.,* Fusion Tech. **18** 461 (1990).
[17] E.D. Fredrickson, N. Gorelenkov, C.Z. Cheng, *et al.*, Phys. Rev. Lett. **87**, (2001) 145001.
[18] R V Budny, Nucl. Fusion **34** (1994) 1247.
[19] N.N. Gorelenkov, C.Z. Cheng, Phys. Plasmas **2** (1995) 1961.
[20] S.M. Mahajan , D.W. Ross, Phys. Fluids **26** (1983) 2561.
[21] B. Coppi, S. Cowley, R. Kulsrud, P. Detragiache, and F. Pegoraro, Phys. Fluids **29**, (1986) 4060.
[22] N.N. Gorelenkov, C.Z. Cheng, Nucl. Fusion **35**, (1995) 1743.
[23] E.D. Fredrickson, N. N. Gorelekov and J. Menard, Phys. of Plasmas **11** (2004) 3653.
[24] N.N. Gorelenkov, E. Fredrickson, E. Belova, C.Z. Cheng, *et al.*, Nucl. Fusion, **43** (2003) 228.
[25] E.V. Belova, *et al.,* Phys. Plasmas **10** 3240 (2003).
[26] C.Z. Cheng and N.N. Gorelenkov, Phys. Plasmas, to appear in Phys. Plasmas (2004).